Available online at www.sciencedirect.com
SCIENCE DIRECT®
PERGAMON
Renewable Energy 28 (2003) 1729–1740
RENEWABLE ENERGY
www.elsevier.com/locate/renene

Monolithic crystalline multijunction solar cell development and analysis at the US Air Force research laboratory

C.S. Mayberry [a,*], K.C. Reinhardt [a], T.L. Kreifels [b]

[a] *Spacecraft Component Technologies Branch, Air Force Research Laboratory, AFRL/VSSV Space Vehicles Directorate , 87117-5776 Kirtland Air Force Base, NM, USA*
[b] *Space and Aeronautics Technology Division, Jackson and Tull, 87106 Albuquerque, NM, USA*

Received 11 September 2002; accepted 1 October 2002

Abstract

As satellite payload electrical power system requirements continue to grow, satellite systems employing flat panel arrays have reached limits set by either on-orbit dynamics that limit the size and shape of the deployed array, mass constraints set by the launch vehicle, or by the limits set by the volume constraints of the launch shroud. This has caused several satellite programs to approach power margin limits early in the design cycle, and to either compromise on satellite capabilities or perform costly redesigns. A very leveraging parameter for raising satellite power levels and reducing costs is the efficiency of the solar cells employed by satellite systems. State of the art efficiencies have reached 26.5% efficiency at load, and 30.1% for prototype cells, and solar arrays using GaAs based multijunction solar cells have achieved deployed solar array power densities of 70 W/kg and stowed volume power densities of 8 kW/m^3. A simplified approach to the unwieldy dark current electrical analysis of multijunction solar cells has been developed, correlated with the performance of dual and triple junction solar cells, and explains ideality factors and reverse saturation currents that appear large. It was found that introducing a fourth junction with modest performance could raise the efficiency of multijunction solar cells to 31.5% efficiency at load, raise total power levels to 22 kW, raise the power densities to 100 W/kg and 9 kW/m^3 with no impact to the configuration or operation of satellite solar arrays.
Published by Elsevier Science Ltd.

* Corresponding author. Tel.:+1-505-846-0499; fax: +1-505-846-9900.
E-mail address: mayberry@plk.af.mil (C.S. Mayberry).

0960-1481/03/$ - see front matter Published by Elsevier Science Ltd.
doi:10.1016/S0960-1481(02)00215-X

Report Documentation Page

Form Approved
OMB No. 0704-0188

1. REPORT DATE	2. REPORT TYPE	3. DATES COVERED
SEP 2003		**-**

4. TITLE AND SUBTITLE	5a. CONTRACT NUMBER
Monolithic crystalline multijunction solar cell development and analysis at the US Air Force Research Laboratory	5b. GRANT NUMBER
	5c. PROGRAM ELEMENT NUMBER
6. AUTHOR(S)	5d. PROJECT NUMBER
C Mayberry*; K Reinhardt*; T Kreifels	5e. TASK NUMBER
	5f. WORK UNIT NUMBER
7. PERFORMING ORGANIZATION NAME(S) AND ADDRESS(ES)	8. PERFORMING ORGANIZATION REPORT NUMBER
Jackson and Tull,1601 SE Randolph Rd,Albuquerque,NM,87106	
9. SPONSORING/MONITORING AGENCY NAME(S) AND ADDRESS(ES)	10. SPONSOR/MONITOR'S ACRONYM(S)
	11. SPONSOR/MONITOR'S REPORT NUMBER(S)

12. DISTRIBUTION/AVAILABILITY STATEMENT

Approved for public release; distribution unlimited

13. SUPPLEMENTARY NOTES

14. ABSTRACT

As satellite payload electrical power system requirements continue to grow, satellite systems employing flat panel arrays have reached limits set by either on-orbit dynamics that limit the size and shape of the deployed array, mass contraints set by the launch vehicle, or by the limits set by the volume constraints of the launch shroud. This has caused several satellite programs to approach power margin limits early in the design cycle, and to either compromise on satellite capabilities or perform costly redesigns. A very leveraging parameter for raising satellite power levels and reducing costs is the efficiency of the solar cells employed by satellite systems. State of the art efficiencies have reached 26.5% efficiency at load, and 30.1% for prototype cells, and solar arrays using GaAs based multijunction solar cells have achieved deployed solar array power densities of 70 W/kg and stowed volume power densities of 8 kW/m{sup 3). A simplified approach to the unwieldy dark current electrical analysis of multijunction solar cells has been developed, correlated with the performance of dual and triple junction solar cells, and explains ideality factors and reverse saturation currents that appear large. It was found that introducing a fourth junction with modest performance could raise the efficiency of multijunction solar cells to 31.5% efficiency at load, raise total power levels to 22 kW, raise the power densities to 100 W/kg and 9 kW/m{sup 3} with no impact to the configuration or operation of stellite solar arrays.

15. SUBJECT TERMS

16. SECURITY CLASSIFICATION OF:			17. LIMITATION OF ABSTRACT	18. NUMBER OF PAGES	19a. NAME OF RESPONSIBLE PERSON
a. REPORT	b. ABSTRACT	c. THIS PAGE			
unclassified	**unclassified**	**unclassified**		**13**	

Nomenclature

A	ideality factor, amps
A_c	apparent ideality factor
I	electronic current
I_{diff}	diffusion current through diode
I_0	reverse saturation current
I_{oc}	apparent reverse saturation current
I_{rec}	recombination current through diode
I_{tunn}	tunneling current through diode
K_B	Boltzmann's constant
q	electronic charge
T	junction temperature
V	voltage

1. Introduction

Commercial satellite bus systems have reached as high as 15 kW with Lockheed Martin Corporation's A2100 Line bus and 18 kW with the BSS 702 configuration. These high power levels are to a large extent enabled by increasingly more efficient monolithic crystalline multijunction solar cells presently being offered by Spectrolab Inc. and Emcore Corporation, and are products of Air Force Research Laboratory programs that seek to achieve efficiencies as high as 35%. Nevertheless, military communications satellites utilizing commercial buses have pushed the design limits of these buses to the point where power margins have been reduced to near zero early in the design cycle. The consequences of a zero power margin can be costly. Experience with the Communications/Navigation Outage Forecasting System (C/NOFS) satellite system shows that even on small satellites, extensive redesign necessitated by a loss of power margin results in very costly redesigns. Future trends predicted by historical evidence dating back to before 1968 show power levels doubling every 5.5 years. Therefore, it is safe to state that military communications satellite designs will continue to push the performance envelope of satellite buses. The Air Force Research Laboratory (AFRL), in anticipation of these increasing power needs, is responding by continuing to improve the state of the art for monolithic crystalline multijunction solar cells. The goal of AFRL programs are to reduce the cost of satellite missions by preventing launch vehicle step-up due to mass or volume considerations of the launch vehicle, and to enable higher powers with present satellite platforms.

The efficiency of the solar array is a very leveraging parameter with which to effect significant changes to the performance of the solar array. The satellite industry continues to be extremely conservative, and is perhaps more so in light of recent

experiences with the Hughes 702 reflective concentrator array. While AFRL is pursuing a number of revolutionary ideas and innovations with regards to solar array design, the impact of programs that seek to provide drop-in replacement monolithic crystalline cells on standard flat panel arrays are much more readily felt. The Advanced Space Power Generation Group at Kirtland AFB, NM began making impacts to the solar cell industry in 1998 with the Mantech program that produced a number of designs which achieved 24% efficiency with triple junction solar cells based on GaAs technology. In early 1999, a Dual Use Science and Technology Program was undertaken to reach new heights in solar cell performance by integrating a fourth junction into an optimized triple junction design with a bandgap energy of 1.0 eV. The goals of these programs can be seen in Fig. 1 that shows the dramatic improvements even with flat panel arrays with increases in efficiency. The top trace in the figure results from the effect of upgrading the solar cells on an array while keeping the array size constant, and the bottom trace results from keeping the array power constant and capturing the reduced mass obtained from retrofitting upgraded cells.

The pursuit of this four junction solar cell has resulted in substantial improvements to the triple junction solar cell since as part of the program plan to incorporate a fourth junction it was necessary to optimize the performance of the triple junction solar cell. The triple junction solar cell achieved as high as 30.1% with a prototype cell, and the program ultimately uncovered difficulties in development of a 1.0 eV material with good crystal quality. The 1.0 eV material has to match the lattice constant of germanium, have bandgap energy close to 1.0 eV, and match the current of the operating cell. The best candidate 1.0 eV material system for a GaAs based cell has been identified as InGaAsN, a quaternary compound that has reached 9 mA/cm^2 with a goal of 16 mA/cm^2. Device designers have cleverly found a cell configuration that can use InGaAsN material with this present current density in a high voltage/low current cell that also has the advantage of less I^2R loss through the series resistance of the cell. Further designs will require the development of optically

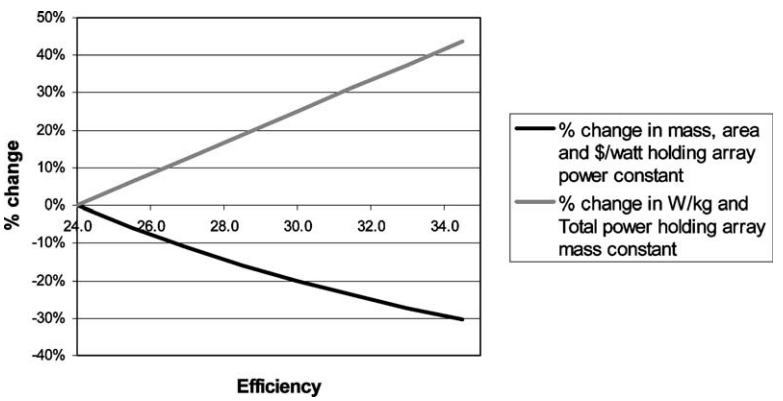

Fig. 1. The percent change in performance of a flat panel array as a function of solar cell efficiency, beginning with 1998 efficiencies.

thin subcells to take advantage of excess current production, balance the production of current among the subcells and provide a better match to the air mass zero (AM0) spectrum. The cycle time from the cell innovations in the laboratory to implementation on a satellite system has been very short if the designs are not disruptive as in recent years since the improvements have been made as optimizations of the standard triple junction solar cell and industry has been able to achieve space qualification on their own. New designs will be more challenging to space qualify, and a myriad of designs are being offered to AFRL for possible development, unfortunately with shrinking budgets AFRL must become more selective. As the electrical analysis of three-, four-, and five-junction solar cells becomes challenging, so does the selection process. Therefore, AFRL has developed a method to electrically analyze the solar cells more efficiently, taking into account recombination, tunneling, and diffusion currents as well as series and shunt resistances, and in this case extending the analysis from triple junction solar cells and examining the performance of a four junction solar cell with a GaInP/GaAs/InGaAsN/Ge configuration.

2. Discussion

The number of recent cell designs of single-crystal multijunction solar cells have established a need to develop a modeling tool to understand better multijunction current–voltage (*I–V*) behavior and predict device performance. Here, we discuss the development of a multijunction dark current model and compare its results with *I–V* data from a triple-junction ($GaInP_2$/GaAs/Ge) solar cell. Our model accounts for all known sources of dark current in individual p–n junctions as well as shunt and series resistance, and is in close agreement with existing triple-junction dark current data. The model was developed to isolate and understand the effect and relative significance of each dark-current mechanism in a specific junction, and the contribution of each junction to overall device performance. Parameters for each subcell were obtained from isotype junctions that contain all optical components of a triple junction cell but with only a single active junction. The isotype data was curve fit to a model that contained tunneling, recombination, and diffusion mechanisms as well as series and shunt resistance. The parameters that were determined from these single junction subcells were then combined in the overall cell model of the triple junction cell and the results compared with data of standard triple junctions cells over the complete range of voltage and current. The model was then extended to predict the influence of an additional junction, in this case, $InGaAsN_2$.

It is well known that dark current in a solar cell is made up of three distinct components: diffusion-limited current, space-charge recombination, and tunneling. Diffusion current follows the renowned Shockley diode model. Recombination-generation current was described by Sah–Noyce–Shockley (SNS) [1]. Tunneling current is treated by Riben and Feucht [2], and again later by Banerjee [3], to describe the higher currents in the low voltage ranges. Each mechanism may be modeled using the photodiode model shown in Fig. 2.

The current–voltage (*I–V*) relationship for the simplified photovoltaic diode is:

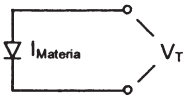

Fig. 2. Simple photodiode model.

$$I = I_0(\exp(qV/Ak_BT)-1) \tag{1}$$

Then, for $V >> k_BT/q$

$$I = I_0 \exp(qV/Ak_BT) \tag{2}$$

where I is the total current across the diode, I_0 is the reverse saturation current, V is the voltage across the junction, A is the junction ideality factor, and q, k_B, and T assume their typical meanings.

The device model developed here uses the simplified diode model to account for electron diffusion, recombination, and tunneling by placing three diodes in parallel each representing an individual mechanism as depicted in Figure 3 and Equation 3 below

$$I_D = I_{diff} \exp(qV/A_{diff}k_BT) + I_{rec} \exp(qV/A_{rec}k_BT) + I_{tunn} \exp(qV/A_{tunn}k_BT) \tag{3}$$

To develop a relation to predict the dominant dark current mechanism as voltage is varied, the simplified diode Eq. (2) was set equal to the three-diode single junction Eq. (3). Both sides of the resulting equation were expanded using a first-order Taylor series approximation about the voltage, V, resulting in the following equations for the apparent ideality factor, A_c, and apparent reverse saturation current, I_{oc}. Note that A_c is a function of the reverse saturation currents and the ideality factors associated with the each dark current mechanism and the operating voltage. The reverse saturation current is now a function of those same parameters and A_c.

$$A_c = \frac{I_{diff\ GaInP_2} \exp(qV_{MPP}/A_{diff\ GaInP_2}k_BT) + I_{rec\ GaInP_2} \exp(qV_{MPP}/A_{rec\ GaInP_2}k_BT) + I_{tunn\ GaInP_2} \exp(qV_{MPP}/A_{tunn\ GaInP_2}k_BT)}{(I_{diff\ GaInP_2}/A_{diff\ GaInP_2}) \exp(qV_{MPP}/A_{diff\ GaInP_2}k_BT) + (I_{rec\ GaInP_2}/A_{rec\ GaInP_2}) \exp(qV_{MPP}/A_{rec\ GaInP_2}k_BT) + (I_{tunn\ GaInP_2}/A_{tunn\ GaInP_2}) \exp(qV_{MPP}/A_{tunn\ GaInP_2}k_BT)} \tag{4}$$

$$I_{oc} = [I_{diff\ GaInP_2} \exp(qV_{GaInP_2}/A_{diff\ GaInP_2}k_BT) + I_{rec\ GaInP_2} \exp(qV_{GaInP_2}/A_{rec\ GaInP_2}k_BT) + I_{tunn\ GaInP_2} \exp(qV_{GaInP_2}/A_{tunn\ GaInP_2}k_BT)] \exp(-qV_{MPP}/A_ck_BT) \tag{5}$$

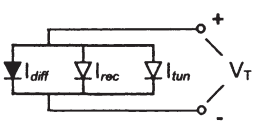

Fig. 3. Photodiode model with recombination, tunneling and diffusion mechanisms.

A closed-form relation for the *I–V* curve can be obtained by inserting A_c and I_{oc} into Eq. (2) resulting in a forward current, I_f, allowing a fit to the entire *I–V* curve

$$I_f = I_{oc} \exp(qV/A_c kT) \tag{6}$$

In the example using typical parameters for a GaAs junction in equations for A_c and I_{oc}, Fig. 4 shows how the ideality factor and reverse saturation current for an ideal junction are monotonically decreasing functions with voltage and results in the semi-log plot of forward diode current having definite changes in slope.

For positive forward voltages, from values slightly greater than zero to approximately 0.3 V, $A_c > 2$ indicating the tunneling dark current mechanism is dominant. Between 0.3 and 0.7 V, the ideality factor has decreased and leveled at approximately $A_c = 2$, indicating that recombination is dominant. Finally, for forward voltages greater than 0.7 V, $A_c = 1$, indicating diffusion is the dominant dark current mechanism. Eq. (6) was used to perform a curve fit to measured data from three isotype cells with active Ge, GaAs, and $GaInP_2$, respectively.

Stirn [4], and Wolf [5], showed that the *I–V* characteristics are not fully described unless series resistance is also included. Therefore, in addition to dark current mechanisms, our model also accounts for series resistance exterior to the active cell and shunt resistance across a material junction as shown in Fig. 5. The resistances account for the increased current at low voltages and the roll off at relatively high voltages.

Using (6), with the addition of terms for shunt and series resistance, a curve fit to measured data from three isotype cells with active Ge, GaAs, and $GaInP_2$ junctions was performed. Fig. 6 illustrates good agreement between the data taken from these cells and the model.

To extend the model to a multijunction cell configuration, a closed-form expression for series connected junctions was derived using the high voltage assump-

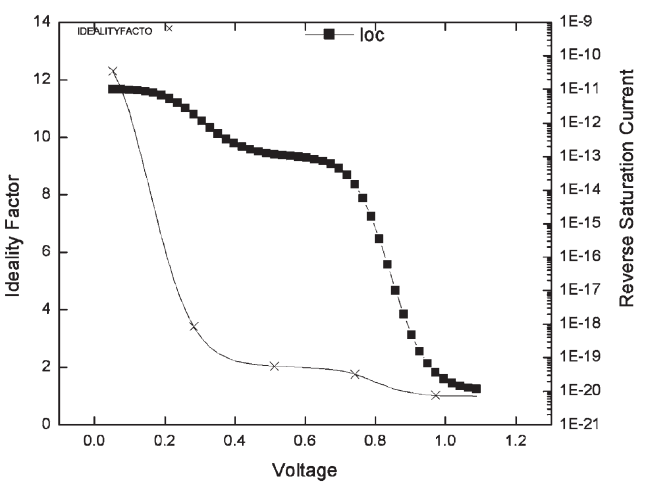

Fig. 4. The ideality factor and reverse saturation current that would be found from fitting the simple diode equation to solar cell dark *I–V* data.

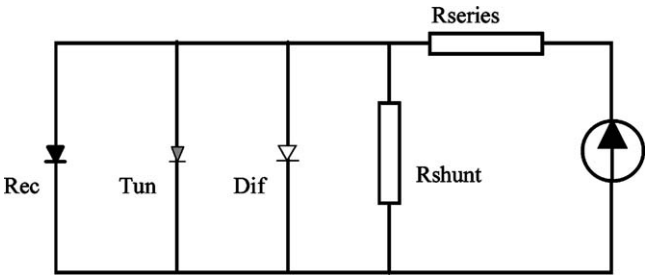

Fig. 5. Dark current model of solar cell depicting current mechanisms and parasitic resistances.

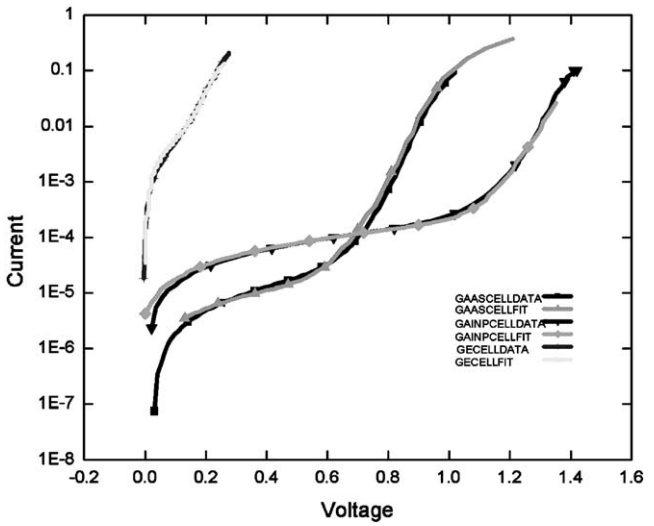

Fig. 6. Curve fits of (6) to data sets corresponding to isotype cells of three junction devices.

tion. Saturation currents and ideality factors were initially calculated by assuming each p–n junction behaved as a single diode with one ideality factor resulting from the combined effects of diffusion, recombination, and tunneling as shown in Fig. 7.

As was shown in previous paper [6], this approach yielded an overall expression for current as a function of device voltage

$$I = I_{\mathrm{GaInP_2}}^{(A_{\mathrm{GaInP_2}}/A_{\mathrm{total}})} I_{\mathrm{GaAs}}^{(A_{\mathrm{GaAs}}/A_{\mathrm{total}})} I_{\mathrm{Ge}}^{(A_{\mathrm{Ge}}/A_{\mathrm{total}})} \exp(qV/A_{\mathrm{total}}k_{\mathrm{B}}T) \tag{7}$$

where

$$A_{\mathrm{total}} = A_{\mathrm{GaInP_2}} + A_{\mathrm{GaAs}} + A_{\mathrm{Ge}} \tag{8}$$

and I_{GaInP2} and A_{GaInP2} are the saturation current and ideality factor for the $GaInP_2$ junction, etc., and I and V are the current and voltage across the entire $GaInP_2$/GaAs/Ge triple junction.

Normally, high ideality factors and high reverse saturation currents indicate a poor

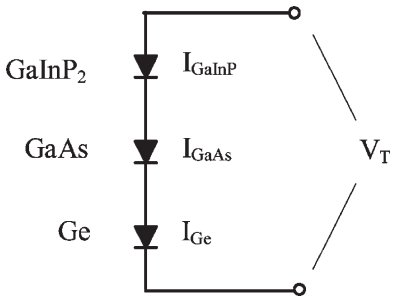

Fig. 7. Simple model of multijunction solar cell.

quality material or junction interface. Eq. (8) explains the apparently high values of overall ideality reported for an otherwise high-quality multijunction sample.

To complete the model, we constructed a series circuit (representing multiple junctions) of parallel circuits (representing multiple dark current mechanisms in each junction), and added shunt resistance across the junction and series resistance across the device, as shown in Fig. 8.

A numerical approach was used to obtain the solution to the circuit shown in Fig. 6. The algorithm selected a current, then computed and summed the voltages associated with the various material systems. This approach allowed a complete curve fit over the entire positive operating range of the device, and allowed tracking of the voltage contributions of each subcell, power losses in parasitic resistances, and current limiting to the lowest subcell current production are observed. What follows are the results of applying the computer model to dark and light *I–V* curves of dual and triple junction cells, and in predicting the performance of a quad junction cell using InGaAsN.

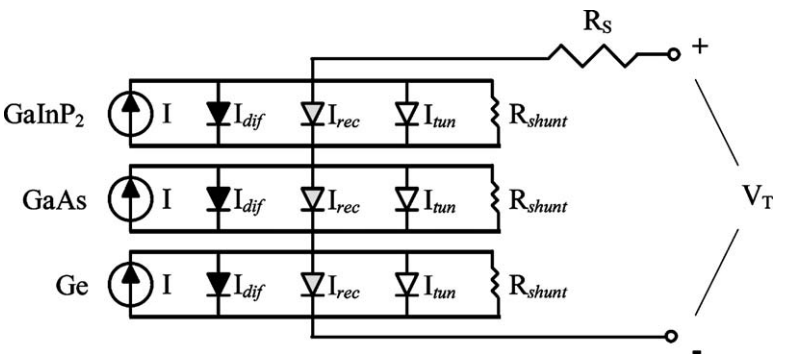

Fig. 8. Complete model of solar cell including individual junction parasitic resistances and dark current mechanisms.

3. Results

Data were taken from a state-of-the-art $GaInP_2$, GaAs, and Ge isotype solar cells. Active device areas ranged from 0.186 to 3.83 cm^2. Contact area but not grid fingers were taken into account. The $GaInP_2$ and GaAs pn junction devices were initially grown by metalorganic chemical vapor deposition (MOCVD), and Ge solar cells grown by diffusion. Dark current measurements were taken using standard equipment from zero voltage to a voltage corresponding to a current limit of 0.1 A. Currents and shunt resistances were normalized to device area to produce current density (J_o, A/cm^2) and resistivities (Ω/cm^2). Light *I–V* measurements were taken using an AM0 solar simulator calibrated with a GaAs balloon standard. In all cases, the range of data included the knee of the diode *I–V* curve.

The results of the model were compared with data taken from a triple junction device. Fig. 9 shows close agreement between the triple junction data and the results from the numerical model using isotype data taken from available isotype cells. The isotype parameters were scaled to the same device area and included the effects of shunt and series resistance. From the model, the voltage at which a subcell contributes to device output voltage can also be determined.

The fourth junction (1.0 eV bandgap InGaAsN) material parameters were estimated. The short circuit current, I_{sc}, was approximated by integrating the product of the quantum efficiency and the solar flux spectrum between the wavelength associated with the bandgap of GaAs (~870 nm) and a 1.0 eV material (1240 nm) assuming a flat quantum efficiency of 92% and yielded 23 mA/cm^2. The open circuit voltage, V_{oc}, was assumed to be 3/4 of the bandgap or 0.75 V. Series and shunt resistances were approximated using results from GaAs and GaInP isotype junctions. At present,

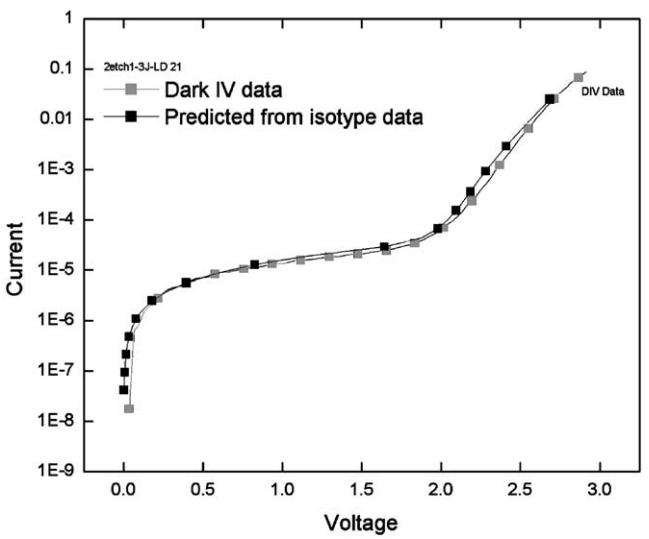

Fig. 9. Data and model agreement for a typical triple junction solar cell.

1.0 eV material systems are nowhere near these values and these represent a starting point for a parametric study.

A parametric study that varied shunt resistance, series resistance, and reverse saturation current was performed for a four junction device. The analysis assumes optimization of the optical thicknesses, windows, contacts, back surface fields, and tunnel junctions. The parameters for the original triple junction were altered to accommodate the fourth junction, and this was mainly a change in the Ge junction since it is assumed that device designers would take advantage of the abundance of current supplied by the Ge subcell at 240 mV and convert a portion of that to a subcell operating at 0.67 V (the 1.0 eV subcell contribution).

The results of this study showed that when series resistance increased much beyond 1 Ω, or shunt resistance was reduced to less than 1 kΩ, or when the reverse saturation current for the device was reduced to less than 1×10^{-9} the efficiency of the four junction device was reduced to that of a triple junction device, the results are just about at breakeven. On the other hand, in order to achieve a step change in performance over and above the triple junction devices that seem to be reaching the point of diminishing returns with respect to the investment in research dollars, the integration of a good quality fourth junction will boost performance with a step change in efficiency of several percent. The graphs in Fig. 10 show how a fourth junction results in boosted efficiency even with a modest crystal quality for the 1.0 eV subcell.

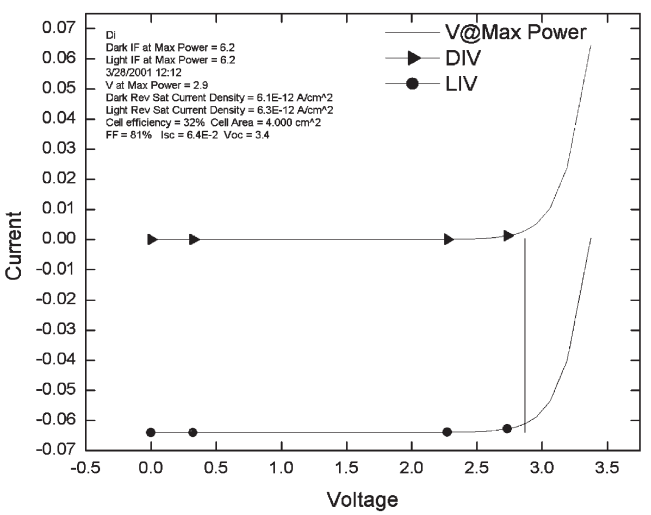

Fig. 10. Analysis of simulated 4J curve using 3J parameters and approximated 4J parameters. The light I-V curve was developed using approximated parameters for the 1.0 eV material system.

4. Conclusions

Recent electrical modeling efforts have shown that the correct approach to gain substantial improvements in the performance multijunction solar cells beyond the substantial gains that seem to be leveling off with triple junction solar cells, will require additional junctions in the form of new material systems, or in splitting subcells to gain additional voltage/power contributions to the cell. A computer model that accounts for all dark current mechanisms, shunt, and series resistance for multiple junctions, and explains some of the variations of ideality factors and reverse saturation currents exhibited by multijunction cells was developed. Dark current mechanisms due to carrier diffusion, carrier recombination, and tunneling via deep defect states within the semiconductor bandgap were characterized within the p–n junctions, and predicted *I–V* curves utilizing the numerical model based on these values yielded plots in good agreement with data taken of state of the art triple junction solar cells developed under US Air Force Research Laboratory programs. The model was extended to a four-junction ($GaInP_2$/GaAs/$InGaAsN_2$/Ge) cell configuration, the two-terminal performance for the four-junction cells was predicted using measured values of I_o and A from isotype junctions of the GaInP, GaAs, and Ge subcells, and approximate parameters for an InGaAsN subcell. The analysis showed that even if modest performance from a 1.0 eV material can be integrated into a triple junction solar cell, the overall efficiency of a 4 J device will reach approximately 32% and is a marked improvement beyond state of the art triple junction solar cells that have achieved essentially 30% as a result of substantial efforts. The analysis showed that the shunt resistance across the fourth junction needs to be at least 10 kΩ and the total reverse saturation current density should be maintained less that 1×10^{-12} A/cm^2 at the maximum power point to allow the fourth junction to impact the maximum power point. Programs at the AFRL are exploring new cell configurations that will make strides in improving the performance of flat panel and concentrator arrays that utilize monolithic crystalline solar cells. The success of these programs will be reported in the next paper.

Acknowledgements

The authors wish to thank Dr Paul Sharps, Emcore Corporation, Dr Nasser Karam and Dr Richard R. King of Spectrolab, Inc., Dr Sarah Kurtz, National Renewable Energy Laboratory (NREL), and John Nocerino, Aerospace Corporation, for their valuable insight and assistance.

References

[1] Sah CT, Noyce RN, Shockley W. Carrier generation and recombination in p–n junctions and p–n junction characteristics. Proc IRE 1957;45:1228–42.

[2] Riben AR, Feucht DL. nGe–pGaAs heterojunctions. Solid State Electron 1966;9:1055–65.

[3] Banerjee S, Anderson WA. Temperature dependence of shunt resistance in photovotaic devices. Appl Physics Lett 7 July 1986;49(1):1038–40.
[4] Stirn RJ. Junction characteriistics of silicon solar cells. Proceedings of the Ninth IEEE Photovoltaics Specialists Conference; 1972. p. 72–82.
[5] Wolf M, Rauchenbach H. Series resistance effects on solar cell measurements. Adv Energy Conver 1963;3:455–79.
[6] Reinhardt KC, Mayberry CS, Lewis BP, Kreifels TL. Multi-junction solar cell iso-junction measurements for junction sensitivity and performance analysis. Proceedings of the 28th IEEE Photovoltaic Specialists Conference; 2000.